Analytical Model for Fictitious Crack Propagation in Reinforced Concrete Beams without Debonding

Ulfkjær, J. P.; Brincker, Rune

Published in:
Proceedings of the International Union of Theoretical and Applied Mechanics (IUTAM) Symposium on Size-Scale Effects in the Failure Mechanisms of Materials and Structures

Publication date:
1996

Document Version
Publisher's PDF, also known as Version of record

24 ANALYTICAL MODEL FOR FICTITIOUS CRACK PROPAGATION IN REINFORCED CONCRETE BEAMS WITHOUT DEBONDING

J.P. ULFKJÆR and R. BRINCKER
Department of Building Technology and Structural Engineering,
Aalborg University, Aalborg, Denmark

Abstract
The non-linear fracture mechanical problem of combined crack growth and reinforcement action is modelled by adopting a simplified fictitious crack model for concrete and a linear elastic-plastic action for the reinforcement. The softening relation of the concrete is assumed to be linear, however, the crack growth is further simplified by introducing a continuous layer of springs at the midsection mainly representing a simplified material response around the fracture zone. In the reinforcement the strain condition is assumed to be equal to the strain condition in the concrete. The important question of debonding between the reinforcement and the concrete is therefore not considered. The model gives closed form solutions for the whole load displacement curve. Further, the model can describe important effects qualitatively correct. For instance the change of behaviour from brittle to ductile when the reinforcement area is increased and from ductile to brittle when the size scale is increased. Experiments are performed with two types of reinforcement, notched and un-notched reinforcements. Comparisons between the model and the experiments show that the assumption of a linear softening relation is not adequate and that the debonding problem should be taken into account.
Keywords: Fictitious Crack Model, Lightly Reinforced, Three Point Bending, Size Effects, Experiments, Debonding.

1 Introduction

Since the invention of the fictitious crack model by A. Hillerborg and M. Modéer in the late 1970´s, [1], a lot of attention has been devoted to this model and other non-linear fracture mechanical models (e.g. The Crack Band Model, [2]). The model is now widely acknowledged and the Norwegian offshore industry has adapted the model in constructing and re-assessing huge concrete offshore platforms as the Draugen Gravity Base Structure with a height of 285 m (1993) [3].

Size-Scale Effects in the Failure Mechanisms of Materials and Structures. Edited by A. Carpinteri.
Published in 1996 by E & FN Spon, 2–6 Boundary Row, London SE1 8HN. ISBN: 0 419 20520 9.

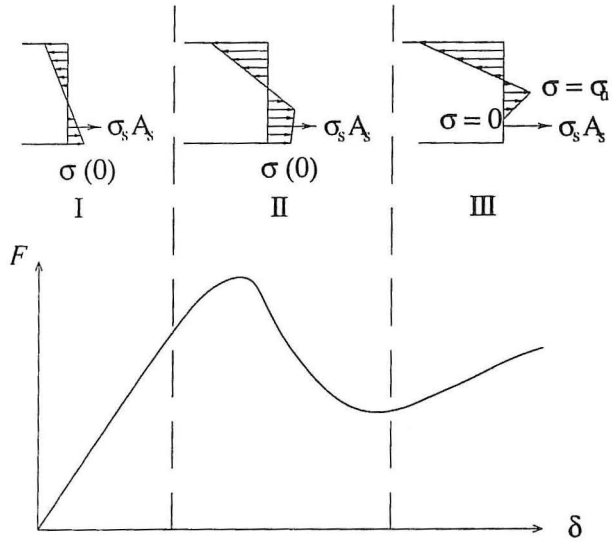

Figure 1. Sketch of the load displacement curve for slightly reinforced concrete beams where the three phases are indicated.

A variety of numerical methods based on the fictitious crack model exists which can be used to predict the load-carrying capacity of plain and reinforced concrete structures, [3][4][5], but there seems to be a lack of simple analytical methods. To the authors' knowledge only one other analytical model exists which describes crack propagation in reinforced concrete beams based on fracture mechanics [6]. The model is based on linear elastic fracture mechanics and assumes that the reinforcement is rigid-perfectly plastic. Thus, this model is applicable to brittle concrete beams.

An analytical model based on the fictitious crack model and a layer of non-linear springs at the midsection of a plain concrete beam in three point bending is developed [7] [8] and also refined for reinforced concrete [9]. The model is here presented in detail and compared with experimental results. Also, the problem of debonding is analysed by testing beams with and without notched reinforcement. It is assumed that the debonding is minimized by using notched reinforcement steel.

2 Basic Assumptions

The fracture process in lightly reinforced concrete beams is assumed to progress as indicated in figure 1. In this model the fictitious crack model is used with the approximations: 1) the local response of the concrete is represented by a thin layer of springs with thickness h due to the crack, 2) the softening relation is linear, 3) the strain in the reinforcement is equal to the strain in the concrete, 4) there is no initial notch or crack, and 5) a single fictitious crack develops at the mid-section. Consider the beam in figure 2 subjected to a rotational controlled load (the rotation φ is the angle between the deflected beam and vertical) with the reinforcement area A_r at the depth r. The reinforcement is assumed to be linear elastic-perfectly plastic as described by the modulus

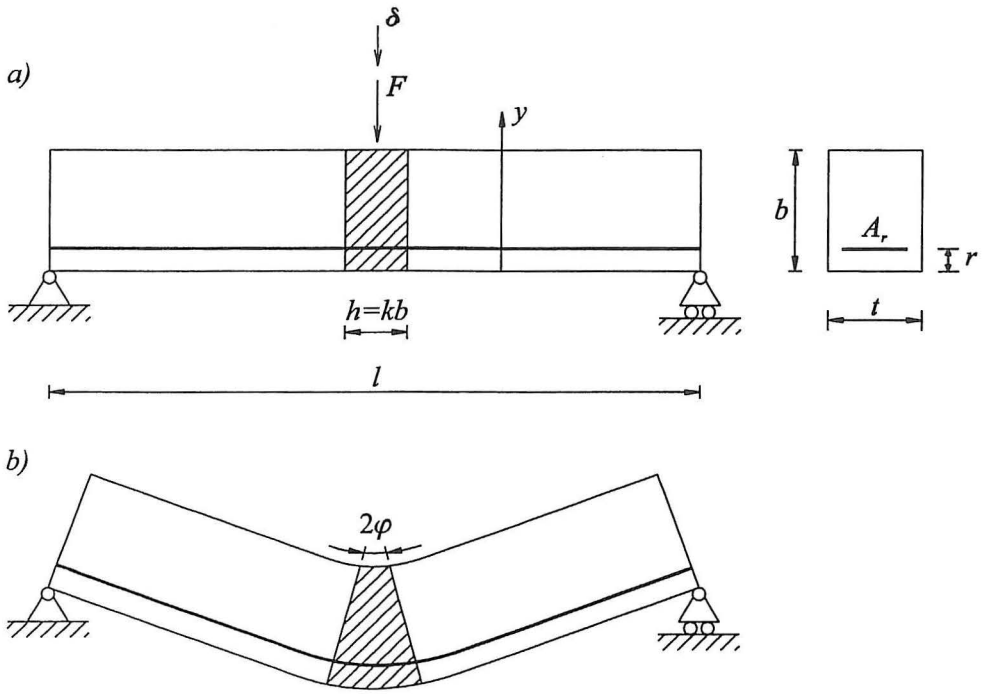

Figure 2. a) The geometry of the considered beam. The hatched area is the layer of non-linear springs. b) The deformed beam, when the elastic deformations in the beam parts outside the layer are neglected.

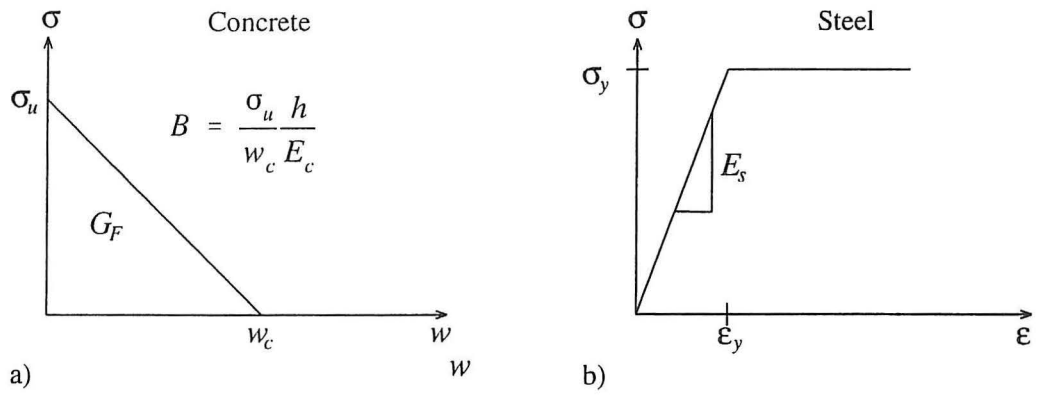

Figure 3. The constitutive relation for a) the concrete and b) the steel.

of elasticity, E_s and the yield stress, σ_y, see figure 3. The concrete is described by the modulus of elasticity and the brittleness number, B. The brittleness number is a parameter including both the material parameters and the beam size. In the present case the brittleness number B is defined as

$$B = \frac{\sigma_u}{w_c}\frac{h}{E_c} = \frac{\sigma_u^2 h}{2G_F E_c} \qquad (1)$$

where E_c is the modulus of elasticity of the concrete, σ_u is the tensile strength of the concrete, G_F is the fracture energy, of the concrete and w_c is the critical crack opening displacement of the concrete, see figure 3. The thickness h of the elastic layer is assumed to be proportional to the beam depth $h = kb$. This assumption has been validated by comparising results for concrete beams with detailed numerical computations where k is varied in order to obtain identical peak loads. These investigations indicated a typical value of $k \simeq 0.5$, Ulfkjær et al. (1990). The calculations are divided into three phases. Phase I): before the tensile strength is reached in the tensile side of the beam, phase II): development of a fictitious crack in the layer, and phase III): crack propagation. The phases and the corresponding stress distributions are indicated in figure 1. Each phase is further divided into two situations: a) the steel remains elastic or b) the steel yields.

The deformation of the layer consists of two contributions. An elastic part v_e and a part w describing the crack opening displacement. The total elengation v is given by $v = v_e + w$.

In phase I $w = 0$. Assuming only rigid body motions of the beam parts outside the layer, it is easily found that in all three phases the total elangation is given by $v = \varphi (c - 2y)$ where c is the size of the compression zone and y is the vertical axis. The size of the compresion zone is determined in phase I by requiring horisontal equilibrium. In phase II and III the size of the compresion zone is determined by considering geometrical similar triangles. By requiring that the stress in the elastic part is equal to the stress in the fictitious crack the crack opening displacement can be determined by using the fact that the stress in the elastic part is $\sigma = E_c \varepsilon_e$ where ε is the strain of the layer given by $\varepsilon = v_e / h$, and the stress in the fictitious crack is determined by the softening relation given by $\sigma(w) = \sigma_u(1 - w/w_c)$. It is thereby possible to describe the stress distribution in the concrete in all three phases.

Considering the concrete model and the reinforcement model the debonding of the steel-concrete interface is not considered. The combined model is constructed simply by taking the simplest possible compatibility condition, namely the reinforcement strain is equal to the concrete strain, i.e. the steel strain in the layer is taken as the layer deformation divided by the layer thickness, and the steel stress can then be computed according to the constitutive condition described in figure 3b.

3 Solutions for the Load-Displacement Curve

In the following the geometrical quantities are made non-dimensional by division by the beam depth, further the corresponding Greek letter is used to indicate a non-dimensional quantity. Reference is also made to section 9 for a full list of notation. Solutions for the case of rigid-body motions for the beam parts outside the layer are given in the following.

3.1 Phase I

In this phase the concrete is linear elastic. Horizontal equilibrium gives the normalized position of the neutral axis (measured from the bottom of the beam) α_η

$$\alpha_\eta = \frac{1}{2}\left(\frac{1 + 2\zeta\rho\alpha_r}{1 + \zeta\rho}\right) \text{ for } \epsilon_s \le \epsilon_y$$
$$\alpha_\eta = \frac{1}{2}\left(1 - \rho\frac{\sigma_y}{\sigma_u}\frac{1}{\theta}\right) \text{ for } \epsilon_s > \epsilon_y \tag{2}$$

where $\zeta = E_s / E_c$ is the flexibility ratio between steel and concrete, $\rho = A_r/td$ is the reinforcement ratio, $\alpha_r = r/d$ is the normalized position of the reinforcement, $\theta = \varphi E_c/k\sigma_u$ is a normalized rotation and ϵ_s is the steel strain. The equivalent non-dimensional moment, $\mu = 6M/td^2\sigma_u$, where $M = 1/4\ Fl$ is the bending moment and F is the force, becomes

$$\mu(\theta) = \theta(4 - 6\alpha_\eta) - 6\frac{\sigma_s(\theta)}{\sigma_u}\rho\alpha_r \tag{3}$$

where σ_s is the steel stress. Thus, the moment rotation curve is linear in phase I if the steel is not yielding, and bi-linear if the steel yields. Phase I ends when the strain at the bottom equals $\epsilon_u = \sigma_u / E_c$ yielding the following condition to the normalized rotation

$$\theta \le \frac{1}{2\alpha_\eta} \tag{4}$$

3.2 Phase II

In phase II the fictitious crack develops. The size of the elastic tensile zone is found by the condition that the strain at the fictitious crack tip is ϵ_u giving $\alpha_\eta = 1/2\theta$. The position of the neutral axis is determined by taking horizontal equilibrium giving the non-dimensional size of the fictitious crack $\alpha_f = a_f / d$

$$\alpha_f = (1 + \zeta\rho)(1 - B) \pm \sqrt{(1 + \zeta\rho)^2(1 - B)^2 - (1 - B)\left((1 + 2\zeta\rho\alpha_r) + \frac{1}{\theta}(1 + \zeta\rho)\right)} \text{ for } \epsilon_s \le \epsilon_y$$
$$\alpha_f = (1 - B) \pm \sqrt{\frac{1}{\theta}(1 - B)\left(1 + \frac{\sigma_y}{\sigma_u}\rho\right)} \text{ for } \epsilon_s > \epsilon_y \tag{5}$$

and the equivalent moment becomes

$$\mu(\theta) = \theta\left(\frac{2\alpha_f(\theta)^3}{1 - B} - 6\alpha_f(\theta) + 4\right) - 3 + 6\frac{\sigma_s(\theta)}{\sigma_u}\rho\alpha_r \tag{6}$$

Which is completely equivalent to the plain concrete model [8] except for the last term taking the steel into account.

3.3 Phase III

In phase III the real crack starts growing. The size of the elastic tensile zone is as in phase II $\alpha_\eta = 1/2\theta$. By considering similar triangles the non-dimensional size α_f of the fictitious crack is determined as

$$\alpha_f = \left(\frac{1 - B}{B}\right)\frac{1}{2\theta} \tag{7}$$

Again this is equivalent to the plain concrete beam. The normalized length of the real crack, α, is determined by requiring horizontal equilibrium.

$$\alpha = 1 + \zeta\rho - \frac{1}{2B\theta} \pm \sqrt{\zeta\rho(\zeta\rho + 2(1 - \alpha_r)) + B\left(\frac{1}{2B\theta}\right)^2} \quad \text{for } \epsilon_s \le \epsilon_y$$

$$\alpha = 1 - \frac{1}{2B\theta} \pm \sqrt{2\rho\frac{\sigma_y}{\sigma_u}\frac{1}{2\theta} + B\left(\frac{1}{2B\theta}\right)^2} \quad \text{for } \epsilon_s > \epsilon_y \tag{8}$$

and the equivalent moment becomes

$$\mu(\theta) = \theta\left(4 - 6\left(\frac{1}{2B\theta} + \alpha\right)\right) + \theta\left(\frac{2(\alpha + \alpha_f)^2 - 2B\alpha^3}{1 - B}\right) + 6\frac{\sigma_s}{\sigma_u}\rho\alpha_r \tag{9}$$

3.4 Elastic Deformations

Elastic deformations in the beam parts outside the elastic layer are allowed for by subtracting the elastic deformation $\mu(\theta)$ from the elastic layer leaving only deformations due to crack growth and then adding the elastic deformations of the whole beam using a solution for an elastic beam with a concentrated force given by [11]. The central elastic beam deflection is

$$\delta_e = \frac{Ml^2}{12EI}\beta(\lambda) \tag{10}$$

where EI is the bending stiffness of the beam, β is a factor describing the influence of the concentrated load $\beta = 1 + 2.85/\lambda^2 - 0.84/\lambda^3$, and λ is the slenderness ratio $\lambda = l/b$. Introducing the elastic rotation

$$\theta_e = 2\frac{\delta_e}{l}\frac{bE}{h\sigma_u} \tag{11}$$

The relation (11) can be written in non-dimensional form

$$\theta_e = \gamma\mu \tag{12}$$

where

$$\gamma = \frac{\beta}{3k\lambda} \tag{13}$$

The effect of the beam flexibility is introduced by adding θ_e and subtracting the deformation of the elastic springs. Thus, the total deformation θ_t is

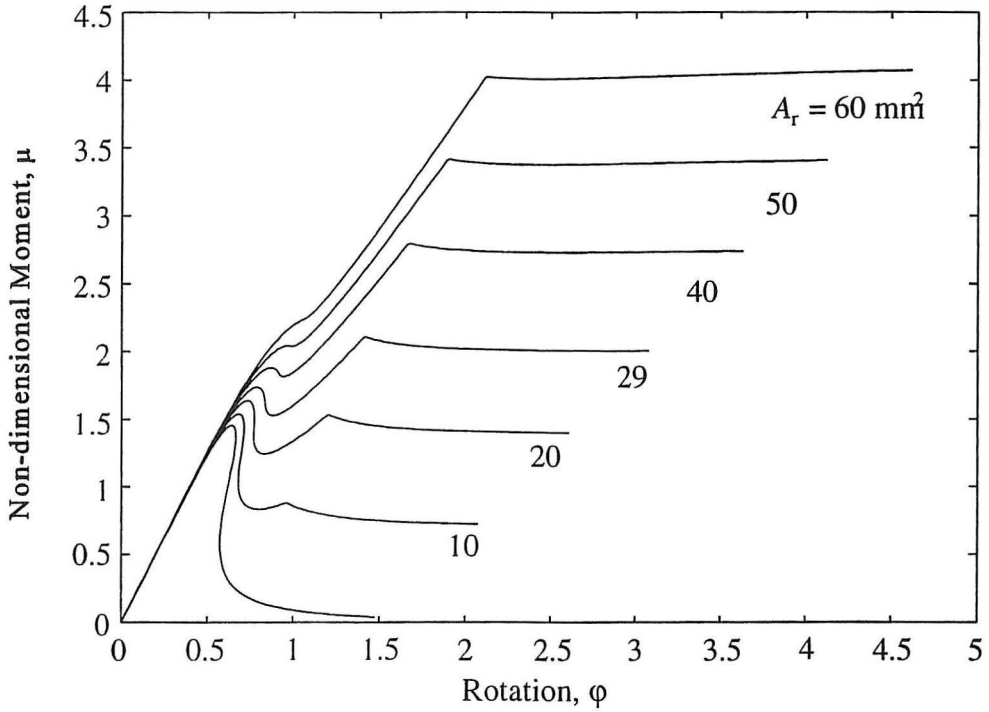

Figure 4. Moment-rotation curves for beams with different reinforcement ratios.

Table 1. Geometry and materials parameters for standard beam.

Beam Depth, b [mm]	200.0
Beam Width, t [mm]	200.0
Beam Length, L [mm]	1600.0
Notch depth, a_i [mm]	0
Position of Steel, r [mm]	10
Specific Fracture Energy, G_F [Nmm/mm^2]	0.1
Concrete Tensile Strength, σ_u [N/mm^2]	3
Modulus of Elasticity, E [N/mm^2]	20000
Brittleness number, B	0.1125
Steel Tensile Strength, σ_y [N/mm^2]	400
Modules of Elastesity for the Steel [N/mm^2]	2.1 E5

$$\theta_t = \theta + \theta_e - \mu = \theta + (\gamma - 1)\mu \tag{14}$$

4 Load-Displacement Curves

A standard beam geometry at different size scales and with different reinforcement ratios are analysed. The geometry and the material parameters for the standard beam are shown in table 1.

Figure 4 shows normalized moment-rotation curves for the standard beam for different reinforcement areas. In figure 5 normalized moment-rotation curves are shown for the standard beam at different size scales but with a constant reinforcement ratio.

The shapes of the curves and the peak moment are seen to be dependent on both the reinforcement area and the size of the structure. Thus, for increasing sizes the

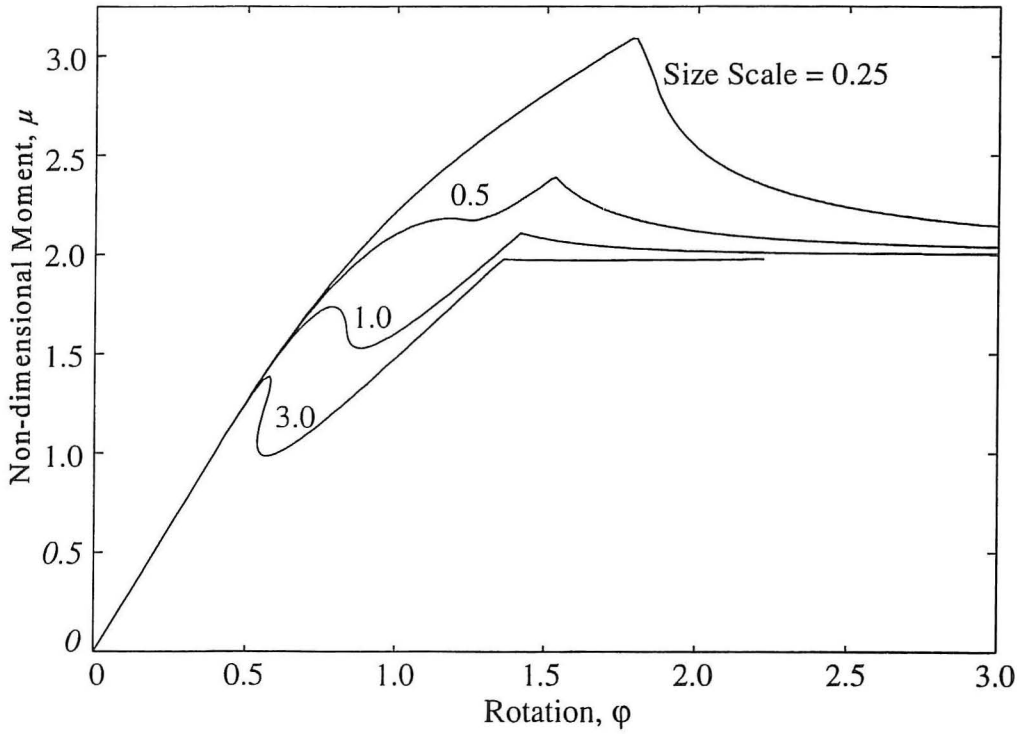

Figure 5. Moment-rotation curves for the reinforced standard beam at different size scales.

maximum non-dimensional moment is decreasing indicating an increasing brittleness and for increasing reinforcement ratios the maximal non-dimensional moment is increasing. For small sizes and large reinforcement ratios the non-dimensional moment at the midsection becomes larger than the moment necessary for initiation of a crack in a neighbouring section. In this case multiple cracking will occur and, thus the assumption of only one crack at the midsection is violated.

5 Experiments

5.1 Materials

Concrete

A high strength concrete with a max. aggregate size of 8 mm was used. the mechanical properties are shown in Table 2

Cylinder compressive strength		Prism splitting strength		Young's modulus	
Mean	S.dev	Mean	S.dev.	Mean	S.dev.
78,3	4.0%	9.30	7.8%	42660	2.5%

Table 2. Mechanical properties of tested concrete, units are [MPa].

Steel

Threaded steel bars were used as reinforcement instead of conventional reinforcement steel. This was done because conventional steel not was available in the small diameters used. Using linear regression the ultimate strength was found as σ_y= 588 MPa with a coefficient of variation of 3.5 %, and the modulus of elasticity was E_s=1.83 10^5MPa with a coefficient of variation of 1.6 %.

Also notched steel bars with two nominal diameters were used d_{nom}= 6.0 mm and 8.0 mm. For each diameter several different notch detphs were considered. Two parabolic relations between the ultimate load and the effective diameter were obtained as $P_u^{(6)}$= - $15.7d_{ef}^4$ + 838.4 $838.4d_{ef}^2$ - 406.3 and $P_u^{(8)}$= - $14.6d_{ef}^4$ + $1191.2d_{ef}^2$ - 3533.2 where P_u is in [N] and d_{ef} is in [mm]. These two expresions are needed to eliminate Weibull effects when designing beams with notched and un-notched reinforcement in order to have the same load carrying capacity.

Specimen

To study the structural size effect the experiments were carried out on 2 different beam geometries (Size A: width and depth: 100 mm and span: 800 mm; Size B width: 100 mm, depth: 200 mm; and span: 800 mm). Here only results for beam size A are presented.

5.2 Testing equipment and procedure

The beams were subjected to three-point bending in a servo-controlled materials testing system. In order to measure the true beam deflection a reference bar was placed on each side of the beam, and the beam deflection was measured as the distance from the load point to the reference bar using two LVDTs.

5.3 Fracture Parameter Results

8 plain concrete beams were tested in three point bending to determine the fracture parameters σ_u and G_F.. The parameters were estimated using a numerical procedure called the direct sub-structure method [11] guessing the shape of the σ-w relation and using the

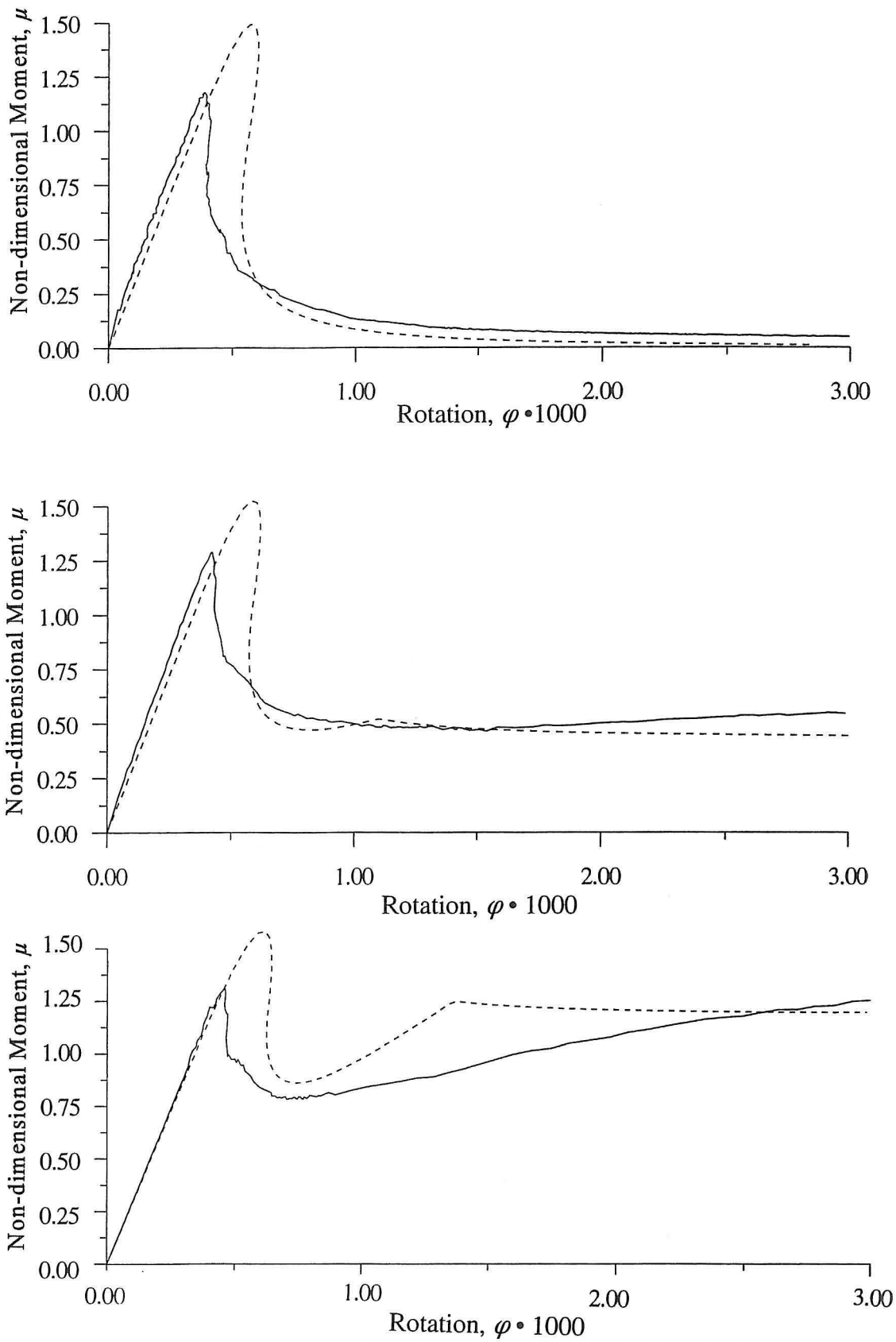

Figure 7. Comparisons between the model- dashed lines and experiments solid lines. For beam type A with diferent reinforcement ratios Top) $A_r = 0$ mm^2 middle) 9.8 mm^2 bottom) 27.7 mm^2

Nelder and Mead scheme, [12] an optimization was carried out to determine the estimates of the two parameters. The method is fully described in [13]. The tensile strength was estimated as 7.39 MPa with a coefficient of variation of 6.4 % and the fracture energy was 0.131 Nmm/mm^2 with a coefficient of variation of 6.9 %.

6 Model evaluation

The material parameters described in the previous section are used as input to the model. When calculating the non-dimensional moment the effective beam depth was used and when calculating the elastic deformations the total beam depth was used. In the following comparison of the model and the experimental results is made. The solid lines are the experiments and the dashed lines are the model curves. In figure 7 the results for series 4 are shown for beam size A with increasing reinforcement area. It is seen that the stifness and the yielding moment are decribed very well whereas the peak moment is calculated to high. This is due to the assumption of a linear softening relation. Instead a bi-linear softening relation should be used, Petersson (1981), Brincker and Dahl (1989). The intermediate phase of the fracture is not described too well, and it is assumed that this is due to the fact that debonding is not taken into account. The yield load is described very well for most of the beams. These results are also general for beam size B.

7 Debonding

The influence of debonding is studied by using notched reinforcement. In this way the stresses in the rebar in sections outside the midsection are small which reduces the debonding in these sections. The difference in the behaviour between the two experiments is therefore mainly attributed to debonding between the rebar and the concrete. Two typical load-displacement curves are shown in figure 8 and it is seen that there is a remarkble difference between the two experiments. The drop in the load after the the first peak is more pronounced for the un-notched beam and the rotational capacity for the un-notched beam is much larger than for the notched beam. Thus, in order to be able to describe the load displacement curve it is necessary to include debonding in the model.

8 Conclusions

A simple analytical model for the response of reinforced beams in bending is developed by combining the fictitious crack model with linear-elastic-perfectly plastic reinforcement action. The method gives explicit solutions for the moment curvature relation and describes transitions from brittle to ductile behaviour with changes in size scale and reinforcement ratio

Experiments were performed on high-strength concrete beams, and the fracture parameters were determined by using an indirect method. The results showed that the assumption of a linear softening relation is too rough, and instead the equations should be derived for a bi-linear softening relation. Further, the experiments showed a significant influence from debonding between reinforcement and concrete.

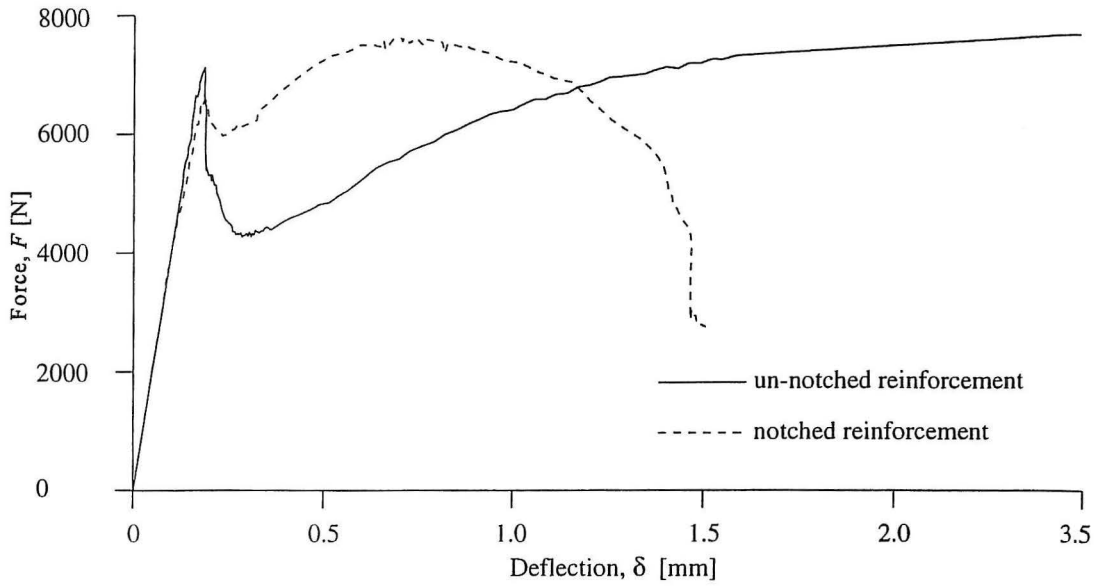

Figure 8. Comparison between two identical beams except for the reinforcement where the solid line is the un-notched reinforcement and the dashed is the notched reinforcement.

9 Acknowledgements

The experimental results presented in the paper are due to work done by Dr. Ole Hededal and Dr. Inger Kroon in connection with their masters thesis which the authors supervised.

10 Notation

The following symbols are used in this paper:

a = real crack length
a_f = fictitious crack length
B = brittleness modulus
b = beam depth
c = size of compresion zone
d_{nom} = the nominal diameter of notched steel
E_c = modulus of elasticity for the concrete
E_s = modulus of elasticity for the steel
G_F = specific fracture energy
h = thickness of layer
I = moment of inertia
k = elasticity coefficient which determines the thickness of the layer
l = beam length
M = cross-sectional moment
w = crack opening displacement

w_c = critical crack opening displacement
v = elongation of layer
v_u = elongation of layer corresponding to the tensile strength
t = beam thickness
α = normalized crack length
α_f = normalized fictitious crack length
α_r = normalized position of the reinforcement
α_η = normalized position of the neutral axis
γ = flexibility coefficient
φ = rotation of beam
θ = normalized rotation
θ_c = normalized rotation that separates phase II and III
λ = slenderness of the beam
μ = normalized cross-sectional moment
ς = stiffness ratio between steel and concrete
σ = axial stresses
σ_u = tensile strength of the concrete
σ_y = tensile strength of the steel
ρ = the reinforcement ratio

11 References

1. Hillerborg, A., Modéer, M. and Petersson, P.E. (1976), Analysis of Crack Formation and Crack Growth in Concrete by Means of Fracture Mechanics and Finite Elements, *Cement and Concrete Research*, pp. 773-782.
2. Bažant Z.P., and Oh, B.H. (1983), Crack Band Theory for Fracture of Concrete, *Materials and Structures*, 16, pp. 155-177.
3. Modéer, M. (1993), Offshore Concrete Platforms in Norway-Materials and Static Analysis, presented at *IUTAM Symposium on 'Fracture of Brittle Disordered Materials: Concrete, Rock and Ceramics'*, September 1993, Queensland, Australia, E & FN Spon, London, pp. 481-494.
4. Modéer, M (1979), A Fracture Mechanics Approach to Failure Analysis of Concrete Materials, *Division of Building Materials, Lund Institute of Technology*, Report TVBM-1001, Lund, Sweden, pp. 1-102.
5. Van Mier, J.G.M. (1989), Other Applications, in *Fracture Mechanics of Concrete Structures- From Theory to Application* (Edited by L. Elfgren), Chapman and Hall, London, pp. 369-381.
6. Bosco, C. and Carpinteri, A. (1990), Fracture Mechanics Evaluation of Minimum Reinforcement in Concrete Structures, in *Application of Fracture Mechanics to Concrete Structures*, Edited by A. Carpinteri, Elsevier Applied Science, Italy, pp. 347-377.
7. Ulfkjær, J.P., Brincker, R. and Krenk, S. (1990), Analytical Model for Complete Moment- Rotation Curves of Concrete Beams in Bending, *in Fracture Behaviour and Design of Materials and Structures*, ECF8 (Edited by D. Firrao), Engineering Materials Advisory Services LTD, Vol II, pp.612-617.
8. Ulfkjær, J.P., Krenk, S. and Brincker, R. (1995), Analytical Model for Fictitious

Crack Propagation in Concrete Beams, *To be published in Journal of Structural Engineering*, Jan 1995.

9. Hededal, O. and Kroon, I.B. (1991), Lightly Reinforced High-Strength Concrete, *M.Sc Thesis at University of Aalborg*, pp. 1-88.
10. Timoshenko, S. (1955), Strength of materials, Part 1, Elementary Theory and Problems, Third Edition, *D. van Nostrand Company Inc.*, New York, p.174.
11. Brincker, R. and Dahl, H. (1989), Fictitious Crack Model of Concrete Fracture, *Magazine of Concrete Research*, 41, No. 147, pp. 79-86.
12 Schittkowski, K. (1985), A FORTRAN subroutine Solving Constrained Non-Linear Programming Problems, *Annals of Operation Research*, Vol. 5, pp. 485-500.
13. Ulfkjær, J.P. and Brincker R. (1993), Indirect Determination of the σ-w Relation of HSC through Three-Point Bending, in *Fracture and Damage of Concrete and Rock, FDCR-2* (Edited by H.P. Rossmanith), Vienna, Austria, E & FN Spon, London, pp.135-144.